INTERNATIONAL JOURNAL OF
NUMERICAL ANALYSIS AND MODELING
Volume 20, Number 5, Pages 597–617

doi: 10.4208/ijnam2023-1026

A FINITE VOLUME ELEMENT SOLUTION BASED ON POSTPROCESSING TECHNIQUE OVER ARBITRARY CONVEX POLYGONAL MESHES

YANLONG ZHANG AND YANHUI ZHOU*

Abstract. A special finite volume element method based on postprocessing technique is proposed to solve the anisotropic diffusion problem on arbitrary convex polygonal meshes. The shape function of polygonal finite element method is constructed by Wachspress generalized barycentric coordinate, and by adding some element-wise bubble functions to the finite element solution, we get a new finite volume element solution that satisfies the local conservation law on a certain dual mesh. The postprocessing algorithm only needs to solve a local linear algebraic system on each primary cell, so that it is easy to implement. More interesting is that, a general construction of the bubble functions is introduced on each polygonal cell, which enables us to prove the existence and uniqueness of the post-processed solution on arbitrary convex polygonal meshes with full anisotropic diffusion tensor. The optimal H^1 and L^2 error estimates of the post-processed solution are also obtained. Finally, the local conservation property and convergence of the new polygonal finite volume element solution are verified by numerical experiments.

Key words. Finite volume element solution, postprocessing technique, convex polygonal meshes, existence and uniqueness, H^1 and L^2 error estimates.

1. Introduction

Finite volume method (FVM) is a popular and practical numerical method for solving partial differential equations, and it is widely used in computational fluid dynamics, computational heat transfer and other fields. The local conservation is an important property of FVM, and it is desirable in multiphase flow in porous media, energy conservation in thermodynamics and many other problems. Finite volume element method (FVEM) is usually regarded as a special type of FVM, where the solution space is the same as the classical finite element method. The mathematical development of FVEM can be found in [18, 20, 37]. For the two dimensional diffusion problems, most existing works of FVEM are only concentrated on triangular meshes (e.g. [1, 5, 6, 7, 9, 34, 36, 39]) or quadrilateral meshes (e.g. [14, 15, 19, 21, 23, 28, 38]). Polygonal meshes offer greater flexibility in mesh generation, merging and refinement, and they have been applied in many fields, such as computational fluid dynamics, topology optimization, analysis of fractured materials and crack propagation and so on. Thus, the construction of FVEM on polygonal meshes is an interesting and important research topic. Recently, [42] proposed a finite volume element method to solve the anisotropic diffusion equation on general convex polygonal meshes, and under the coercivity assumption, the authors proved the optimal H^1 error estimate. To our knowledge, the theoretical analysis of FVEM on arbitrary convex polygonal meshes still lags far behind. For instance, even though for the classical isoparametric bilinear FVEM, the corresponding coercivity result and optimal L^2 error analysis have not been established on arbitrary trapezoidal meshes.

Received by the editors on December 26, 2022 and, accepted on May 8, 2023.
2000 *Mathematics Subject Classification.* 35J25, 65N12, 65N15.
*Corresponding author.

As we all know, since the bilinear form of classical finite element method (FEM) is symmetry, the coercivity result can be easily obtained (e.g. [2, 3]). Once the optimal interpolation error estimate is established, the optimal error analysis (e.g. H^1 and L^2) of FEM can also be proved by some standard techniques (e.g. Aubin-Nitsche). In recent decades, based on various generalized barycentric coordinates, some researchers extend the classical FEM to polygonal meshes, where the generalized barycentric coordinates are studied in [10, 11, 12, 16, 25, 33] for incomplete references. In [30], the polygonal FEMs based on Wachspress, mean value or Laplace generalized barycentric coordinates were developed. For more studies and applications about polygonal finite element method, the readers are referred to [24, 26, 29, 32, 35] and so on. At the same time, [13] (resp. [27]) studied the interpolation error estimates of triangulation, harmonic, Wachspress and Sibson (resp. mean value) coordinates, which is crucial to the optimal error estimates in polygonal FEM and FVEM.

Regrettably, the aforementioned polygonal FEM doesn't satisfy the local conservation property in general. Thus, some researchers try to postprocess the FEM solution to obtain a new FVEM solution with the local conservation property. By postprocessing the continuous Galerkin finite element solution, [43] presented a high order finite volume element solution for the elliptic problem on triangular and quasi-parallelogram meshes, which has the local conservation property and preserves the H^1 and L^2 error estimates. Later, [40] generalized the theoretical results in [43] to the anisotropic diffusion equation on arbitrary trapezoidal meshes. Recently, by introducing some new bubble functions, [41] improved the postprocess technique in [43, 40], such that the new theoretical findings cover arbitrary triangular and convex quadrilateral meshes for the anisotropic diffusion equation with any full diffusion tensor. In addition, there are many other research results for the local conservative method based on FEM, e.g. [4, 8, 17, 22, 31].

Compared with the previous works, this article has several contributions. Firstly, by introducing a unified construction of bubble functions, we establish the existence and uniqueness, optimal H^1 and L^2 error estimates of the post-processed solution for the anisotropic diffusion equation on arbitrary convex polygonal meshes. Secondly, we note that the coercivity result in [42] does not cover general convex polygonal meshes, and the L^2 error estimate of it has not been established. Different from [42], here we present another routine to obtain a new polygonal finite volume element solution for solving the anisotropic diffusion equation, and the stability and convergence are verified on arbitrary convex polygonal meshes.

The rest of this article is organized as follows. In Section 2, we define some notations and introduce the polygonal finite element method based on Wachspress generalized barycentric coordinate. By postprocessing the polygonal finite element solution, in Section 3 we reach a polygonal finite volume element solution, and the local conservation, existence and uniqueness of the post-processed solution are verified in Section 4. The optimal error estimates in H^1 and L^2 norms are proved in Section 5. In Section 6, we present some numerical results to validate the accuracy, local conservation property and mesh flexibility of the proposed method. Some conclusions are given in the last section.

2. A polygonal finite element method

Consider the following anisotropic diffusion problem

$$-\nabla \cdot (\Lambda \nabla u) = f \quad \text{in } \Omega, \tag{1}$$

$$u = g \quad \text{on } \partial\Omega, \tag{2}$$

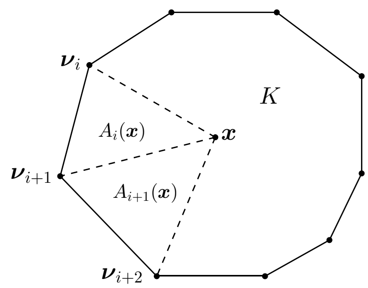

FIGURE 1. Notations of a general convex polygon.

where Ω is an open bounded polygonal domain in $\mathbb{R}^2$, and $f \in L^2(\Omega)$ is the source term. Here Λ is a symmetric and positive definite matrix,

$$\underline{\lambda}\|\boldsymbol{v}\|^2 \leq \boldsymbol{v}^T\Lambda\boldsymbol{v} \leq \overline{\lambda}\|\boldsymbol{v}\|^2, \quad \forall\, \boldsymbol{v} \in \mathbb{R}^2, \tag{3}$$

where $\underline{\lambda}$, $\overline{\lambda}$ are two positive constants, and $\|\cdot\|$ is the Euclidean norm. For simplicity of the proof, we assume the Dirichlet boundary condition $g = 0$ in the theoretical analysis.

2.1. The primary mesh and Wachspress shape function. In order to introduce the primary mesh, we firstly present the following notations and assumptions.

- $\mathcal{M}$, the set of disjoint polygonal cells, satisfying $\overline{\Omega} = \cup_{K\in\mathcal{M}}\overline{K}$. K, a generic cell in $\mathcal{M}$, is an open and connected subset of Ω. Throughout, we suppose that K is strictly convex in the sense that all interior angles of K are less than π. $\boldsymbol{x}_K$, h_K and ρ_K denote the position vector of the cell center, the diameter of K and the radius of the largest circle inscribed in K respectively, and $h = \max_{K\in\mathcal{M}} h_K$.
- $\mathcal{E}$, the set of disjoint edges. σ, a generic edge of $\mathcal{E}$, is an open line segment.
- $\mathcal{V}$, the set of vertices. $\boldsymbol{\nu}$, a generic vertex of $\mathcal{V}$, is a vertex of the cell $K \in \mathcal{M}$. We also use the same notation $\boldsymbol{\nu}$ to denote the position vector of the vertex $\boldsymbol{\nu}$, and let $\mathcal{V}^{int} = \mathcal{V} \cap \Omega$ be the interior vertices of Ω.

Based on the above notations, the *primary mesh* $\mathcal{T}_h$ of Ω is defined by the triplet $(\mathcal{M}, \mathcal{E}, \mathcal{V})$. In this paper, we suppose that the primary mesh is *conforming* in the sense that the intersection of the enclosures of any two cells in $\mathcal{M}$ is either empty or a common vertex or a common edge.

Next, we begin to construct the Wachspress shape functions on a single polygonal cell $K \in \mathcal{M}$. Assume that $\boldsymbol{\nu}_i$ $(i = 1, \cdots, n_K)$ are the n_K vertices of K, see Figure 1, where the vertices are arranged by anticlockwise. In the following discussion, if there is no ambiguity, we will drop the subscript K in n_K for simplicity of exposition. For any $\boldsymbol{x} \in \overline{K}$, let $A_i(\boldsymbol{x})$ be the area of the triangle with vertices $\boldsymbol{x}$, $\boldsymbol{\nu}_i$ and $\boldsymbol{\nu}_{i+1}$, namely

$$A_i(\boldsymbol{x}) = \frac{1}{2}\left(\boldsymbol{\nu}_{i+1} - \boldsymbol{\nu}_i\right)^T \mathcal{R}\left(\boldsymbol{x} - \boldsymbol{\nu}_i\right), \quad \forall\, \boldsymbol{x} \in \overline{K}, \tag{4}$$

where

$$\mathcal{R} = \begin{pmatrix} 0 & 1 \\ -1 & 0 \end{pmatrix}.$$

Here and hereafter, without special mention, the subscripts such as i and j related to the vertices of K will be understood as periodic ones with period n such that $\boldsymbol{\nu}_0 = \boldsymbol{\nu}_n$, $\boldsymbol{\nu}_{n+1} = \boldsymbol{\nu}_1$. It is easy to verify that $A_i(\boldsymbol{x})$ is a linear scalar function with respect to $\boldsymbol{x}$. Moreover, we suppose that $w_i(\boldsymbol{x})$ is the so-called weight function associated with $\boldsymbol{\nu}_i$. In particular, the following weight functions are proposed by Wachspress [33]

$$w_i(\boldsymbol{x}) = A_i(\boldsymbol{\nu}_{i-1}) \prod_{j \neq i-1,i} A_j(\boldsymbol{x}), \quad i = 1, \cdots, n, \tag{5}$$

which are the polynomials of degree not greater than $n-2$ with respect to $\boldsymbol{x}$. Then, the Wachspress shape function associated with $\boldsymbol{\nu}_i$ on K is defined by

$$\phi_i(\boldsymbol{x}) = \frac{w_i(\boldsymbol{x})}{\sum_{j=1}^n w_j(\boldsymbol{x})}, \quad \boldsymbol{x} \in \overline{K}. \tag{6}$$

The properties of Wachspress shape functions are similar to the classical nodal basis functions of Lagrange type on triangular or quadrilateral cells, here we list some of them.

Proposition 1. *([12, 25]) Assume that K is a strictly convex polygon. Let the weight function $w_i(\boldsymbol{x})$ and shape function $\phi_i(\boldsymbol{x})$ be defined by* (5) *and* (6)*, respectively. Then, we have*

$$\phi_i(\boldsymbol{x}) \in C^\infty(K), \quad 1 \le i \le n,$$

$$\phi_i(\boldsymbol{x}) > 0, \quad 1 \le i \le n, \quad \forall \boldsymbol{x} \in K,$$

$$\sum_{i=1}^n \phi_i(\boldsymbol{x}) = 1, \quad \forall \boldsymbol{x} \in K, \tag{7}$$

$$\sum_{i=1}^n \phi_i(\boldsymbol{x}) \boldsymbol{\nu}_i = \boldsymbol{x}, \quad \forall \boldsymbol{x} \in K. \tag{8}$$

Moreover, $\phi_i(\boldsymbol{x})$ has a unique continuous extension to ∂K, satisfying (7)*,* (8) *and $\phi_i(\boldsymbol{x}) \ge 0$ for all $\boldsymbol{x} \in \overline{K}$, and it is linear on each edge of K, satisfying the Lagrange property $\phi_i(\boldsymbol{\nu}_j) = \delta_{ij}$, $1 \le i, j \le n$, where δ_{ij} denotes the Kronecker delta.*

Proposition 2. *([12, 13]) The Wachspress shape functions on convex polygons have the invariance property: if the transformation $T : \mathbb{R}^2 \to \mathbb{R}^2$ is a translation, rotation, reflection, uniform scaling, or combination of these, then $\phi_i(\boldsymbol{x}) = \widehat{\phi}_i(T(\boldsymbol{x}))$, where $\widehat{K} = T(K)$ and $\widehat{\phi}_i$ is the Wachspress shape function defined on $\widehat{K}$.*

Once the Wachspress shape functions ϕ_i $(i = 1, \cdots, n)$ are well defined in each cell K, then by a way similar to the construction of the classical P_1 (resp. Q_1) nodal basis functions of Lagrange type on triangular (resp. quadrilateral) meshes, we can extend ϕ_i to the whole domain $\overline{\Omega}$. In particular, let $\phi_{\boldsymbol{\nu}}(\boldsymbol{x})$, $\boldsymbol{x} \in \overline{\Omega}$ be the Wachspress shape function associated with the vertex $\boldsymbol{\nu} \in \mathcal{V}$, then for any vertex $\boldsymbol{\nu}' \in \mathcal{V}$, we have

$$\phi_{\boldsymbol{\nu}}(\boldsymbol{\nu}') = \begin{cases} 1, & \text{if } \boldsymbol{\nu}' = \boldsymbol{\nu}, \\ 0, & \text{if } \boldsymbol{\nu}' \neq \boldsymbol{\nu}. \end{cases}$$

Obviously, we have $\phi_{\boldsymbol{\nu}} \in C(\overline{\Omega})$.

2.2. A finite element method on polygonal meshes. With respect to the primary mesh $\mathcal{T}_h$, the *finite element space* for (1) and (2) is defined by

$$U_h = \mathrm{Span}\{\phi_{\boldsymbol{\nu}} : \boldsymbol{\nu} \in \mathcal{V}^{int}\}.$$

It is easy to verify that $U_h \subset H_0^1(\Omega)$. Moreover, there holds

$$u_h = \sum_{\boldsymbol{\nu} \in \mathcal{V}^{int}} u_h(\boldsymbol{\nu})\phi_{\boldsymbol{\nu}}, \quad \forall\, u_h \in U_h.$$

The polygonal finite element method for solving (1) and (2) is to find $u_h \in U_h$, such that

$$a(u_h, v_h) = (f, v_h), \quad \forall\, v_h \in U_h, \tag{9}$$

where

$$a(u_h, v_h) = \int_\Omega (\Lambda \nabla u_h) \cdot \nabla v_h \,\mathrm{d}x\mathrm{d}y, \quad (f, v_h) = \int_\Omega f v_h \,\mathrm{d}x\mathrm{d}y.$$

Let the semi-norm and norm of Sobolev space $H^m(\mathcal{D})$ be denoted as $|\cdot|_{m,\mathcal{D}}$ and $\|\cdot\|_{m,\mathcal{D}}$, and when $\mathcal{D} = \Omega$ we omit the subscript Ω. By (3), we find that

$$a(u_h, u_h) \ge \underline{\lambda} |u_h|_1^2, \quad \forall\, u_h \in U_h. \tag{10}$$

Thus, the coercivity result of polygonal finite element bilinear form $a(\cdot,\cdot)$ is verified by noticing (10), and then the existence and uniqueness of (9) can be obtained immediately.

Let the interior angle at the vertex $\boldsymbol{\nu}_i$ be denoted as α_i, i.e., $\alpha_i = \angle \boldsymbol{\nu}_{i-1}\boldsymbol{\nu}_i\boldsymbol{\nu}_{i+1}$. Then, we introduce the geometric assumptions below.

- (**G1**) There exists a positive constant γ^* such that
$$\frac{h_K}{\rho_K} < \gamma^*, \quad \forall\, K \in \mathcal{M}.$$
- (**G2**) There exists a positive constant d_* such that
$$\frac{1}{h_K} \min_{i \ne j} \|\boldsymbol{\nu}_i - \boldsymbol{\nu}_j\| > d_*, \quad \forall\, K \in \mathcal{M}.$$
- (**G3**) There exists a positive constant α^* such that
$$\max_{1 \le i \le n} \{\alpha_i\} < \alpha^* < \pi, \quad \forall\, K \in \mathcal{M}.$$
- (**G4**) There exists a positive constant α_* such that
$$\min_{1 \le i \le n} \{\alpha_i\} > \alpha_*, \quad \forall\, K \in \mathcal{M}.$$
- (**G5**) There exists a positive constant n^* such that $n < n^*$.

Proposition 3 (Proposition 4 in [42], Proposition 4 in [13])**.** *For the geometric assumptions* (**G1**)*-*(**G5**)*, we have the following results:*

(1) (**G2**) *and* (**G3**) *imply* (**G1**)*; (2)* (**G1**) *implies* (**G4**)*; (3)* (**G2**) *or* (**G3**) *implies* (**G5**)*.*

Proposition 3 implies that (**G2**) and (**G3**) are basic ones. Moreover, based on the two assumptions (**G2**) and (**G3**), we have the following interpolation error estimates. Next, we use $A \lesssim B$ (resp. $A \gtrsim B$) to denote $A \le CB$ (resp. $A \ge CB$), where C is a positive constant and independent of K and h. Moreover, $A \sim B$ denotes that we have both $A \lesssim B$ and $A \gtrsim B$.

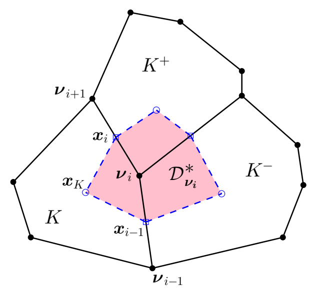

FIGURE 2. The construction of dual cell.

Lemma 1. *Let $u_I \in U_h$ be the Lagrange interpolation of u, satisfying $u_I(\boldsymbol{\nu}) = u(\boldsymbol{\nu})$, $\forall\, \boldsymbol{\nu} \in \mathcal{V}$. Then, under the two geometric assumptions* (**G2**) *and* (**G3**)*, we have the following interpolation error estimates*

$$\|u - u_I\|_{m,K} \lesssim h_K^{2-m} |u|_{2,K}, \quad m = 0, 1, 2, \quad \forall\, u \in H^2(K). \tag{11}$$

Proof. If $m = 0, 1$ (resp. $m = 2$), then the proof of (11) can be found in Theorem 1 and Corollary 1 in [13] (resp. Theorem 1 in [42]). □

Lemma 2. *Assume that $\mathcal{T}_h$ is a conforming mesh, which consists of general convex polygons, and satisfies the same geometric assumptions of Lemma 1. Let u be the exact solution of* (1) *and* (2)*, and u_h the polygonal finite element solution of* (9)*. Then, if $u \in H^2(\Omega)$, we have the following optimal L^2 and H^1 error estimates*

$$\|u - u_h\|_m \lesssim h^{2-m} \|u\|_2, \quad m = 0, 1. \tag{12}$$

Proof. By using Lemma 1 and the similar discussions (e.g. Aubin-Nitsche technique) for the classical continuous Galerkin finite element method of Lagrange type on triangular or quadrilateral meshes (e.g. [2, 3]), we reach (12). □

3. A finite volume element solution based on postprocessing technique

3.1. The dual mesh. For any $K \in \mathcal{M}$, suppose that $\boldsymbol{x}_K$ is an arbitrary interior point of K and $\boldsymbol{x}_i$ is the midpoint of line segment $\boldsymbol{\nu}_i\boldsymbol{\nu}_{i+1}$ $(i = 1, \cdots, n)$. Connecting the cell center with the edge midpoints, we obtain a subdivision of K, consisting of n quadrilaterals. For each vertex $\boldsymbol{\nu} \in \mathcal{V}$, the dual cell associated with $\boldsymbol{\nu}$ is a polygonal domain surrounding $\boldsymbol{\nu}$ and denoted as $\mathcal{D}^*_{\boldsymbol{\nu}}$. Precisely, if $\boldsymbol{\nu} = \boldsymbol{\nu}_i$ is the $i-$th vertex of K, then the contribution of K to $\mathcal{D}^*_{\boldsymbol{\nu}}$ is the quadrilateral $\boldsymbol{\nu}_i\boldsymbol{x}_i\boldsymbol{x}_K\boldsymbol{x}_{i-1}$. The dual cell associated with the interior vertex $\boldsymbol{\nu}_i$ is shown in Figure 2 for an example.

The *dual mesh* $\mathcal{T}'_h$ consists of all dual cells, given by

$$\mathcal{T}'_h = \{\mathcal{D}^*_{\boldsymbol{\nu}} : \boldsymbol{\nu} \in \mathcal{V}\},$$

and the corresponding *test function space* for FVEM is defined by

$$V_h = \mathrm{Span}\{\psi_{\boldsymbol{\nu}} : \boldsymbol{\nu} \in \mathcal{V}^{int}\},$$

where $\psi_{\boldsymbol{\nu}}$ is the characteristic function on $\mathcal{D}^*_{\boldsymbol{\nu}}$, i.e., $\psi_{\boldsymbol{\nu}}(\boldsymbol{x}) = 1$ if $\boldsymbol{x} \in \mathcal{D}^*_{\boldsymbol{\nu}}$, $\psi_{\boldsymbol{\nu}}(\boldsymbol{x}) = 0$ if $\boldsymbol{x} \notin \mathcal{D}^*_{\boldsymbol{\nu}}$. Moreover, let Π be a linear mapping which maps $u_h \in U_h$ to $u^*_h := \Pi u_h \in V_h$, and satisfies

$$u^*_h(\boldsymbol{\nu}) = u_h(\boldsymbol{\nu}), \quad \forall\, \boldsymbol{\nu} \in \mathcal{V}^{int}. \tag{13}$$

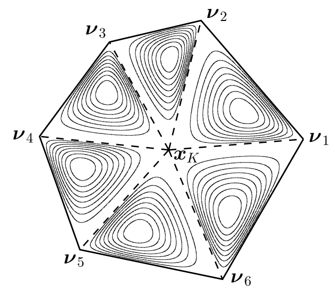

FIGURE 3. The contours of the bubble functions.

If u_h is the polygonal finite element solution of (9), then in general, it does not satisfy the following local conservation property

$$\int_{\partial\mathcal{D}_{\boldsymbol{\nu}}^*} (\Lambda\nabla u_h)\cdot\boldsymbol{n}\,\mathrm{d}s + \int_{\mathcal{D}_{\boldsymbol{\nu}}^*} f\,\mathrm{d}x\mathrm{d}y = 0 \tag{14}$$

for any $\boldsymbol{\nu}\in\mathcal{V}^{int}$, where $\boldsymbol{n}$ denotes the unit normal vector outward to $\partial\mathcal{D}_{\boldsymbol{\nu}}^*$. For example, on triangular meshes, the polygonal finite element solution is identical to the standard P_1 finite element solution since the uniqueness of generalized barycentric coordinates. As a result, u_h doesn't satisfy the local conservation property, even though $n=3$.

However, for the finite volume element solution, it preserves the property (14) on a certain dual mesh (e.g. [18, 20, 37, 42]). In this paper, we postprocess the polygonal finite element solution u_h of (9) to generate a new continuous function $\widehat{u}_h$, such that the new polygonal finite volume element solution satisfies the local conservation property on the dual mesh $\mathcal{T}_h'$, and preserves the optimal H^1 and L^2 error estimates on the primary mesh $\mathcal{T}_h$. For this purpose, a general construction of new n bubble functions for each cell K and a postprocessing algorithm are presented as follows.

3.2. The postprocessing technique. In order to introduce the postprocessing technique, we first introduce the new bubble function ψ_j as below

$$\psi_j = \begin{cases} \lambda_{\boldsymbol{x}_K}\lambda_{\boldsymbol{\nu}_j}^2\lambda_{\boldsymbol{\nu}_{j+1}}, & \text{in } \triangle\boldsymbol{x}_K\boldsymbol{\nu}_j\boldsymbol{\nu}_{j+1}, \\ 0, & \text{otherwise}, \end{cases} \qquad j=1,\cdots,n, \tag{15}$$

where $\lambda_{\boldsymbol{x}_K}$, $\lambda_{\boldsymbol{\nu}_j}$ and $\lambda_{\boldsymbol{\nu}_{j+1}}$ denote three linear nodal basis functions of the triangle $\boldsymbol{x}_K\boldsymbol{\nu}_j\boldsymbol{\nu}_{j+1}$. We plot the contours of six bubble functions for the case $n=6$ in Figure 3. Moreover, in each $K\in\mathcal{M}$, for the polygonal finite element solution u_h of (9), we define the following trilinear form

$$\begin{aligned} R_K(f,u_h,v_h) = &\int_K f(v_h^*-v_h)\,\mathrm{d}x\mathrm{d}y + \int_K (\Lambda\nabla u_h)\cdot\nabla v_h\,\mathrm{d}x\mathrm{d}y \\ &+ \int_{\partial K}\{\Lambda\nabla u_h\}\cdot\boldsymbol{n}(v_h^*-v_h)\,\mathrm{d}s, \end{aligned} \tag{16}$$

where $v_h\in U_h$, and $v_h^*\in V_h$ is the piecewise constant function defined by (13), $\boldsymbol{n}$ denotes the unit normal vector outward to ∂K. $\{\cdot\}$ denotes an averaging operator on ∂K, i.e., for any edge $\sigma = \overline{K}_1 \cap \overline{K}_2$, vectorial function $\boldsymbol{v}$ satisfies

$$\{\boldsymbol{v}\}_\sigma = \frac{1}{2}\left(\boldsymbol{v}|_{\sigma,\overline{K}_1} + \boldsymbol{v}|_{\sigma,\overline{K}_2}\right).$$

Next, we introduce the postprocessing technique. For each $K \in \mathcal{M}$, we define the post-processed solution as

$$\widehat{u}_h = u_h + \sum_{j=1}^{n} c_j \psi_j, \tag{17}$$

where c_j $(j = 1, \cdots, n)$ are some coefficients to be determined. We require that $\widehat{u}_h$ satisfies

$$-\int_{(\partial\mathcal{D}^*_{\boldsymbol{\nu}_i})\cap K} (\Lambda\nabla\widehat{u}_h)\cdot\boldsymbol{n}\,\mathrm{d}s = R_K(f, u_h, \phi_{\boldsymbol{\nu}_i}), \quad i = 1, \cdots, n, \tag{18}$$

$$\sum_{j=1}^{n} \widehat{u}_h(\boldsymbol{y}_j) = \sum_{j=1}^{n} u_h(\boldsymbol{y}_j), \tag{19}$$

where $\boldsymbol{y}_j$ is the barycenter of $\triangle \boldsymbol{x}_K \boldsymbol{\nu}_j \boldsymbol{\nu}_{j+1}$.

Lemma 3. *The equations in* (18) *have linear correlation.*

Proof. In each cell K, by (7) and noticing that $\Lambda\nabla\widehat{u}_h$ is smooth across each edge of $(\partial\mathcal{D}^*_{\boldsymbol{\nu}_i}) \cap K$ (i.e. $\boldsymbol{x}_{i-1}\boldsymbol{x}_K$ and $\boldsymbol{x}_i\boldsymbol{x}_K$), then we find that

$$\sum_{i=1}^{n}\left(R_K(f, u_h, \phi_{\boldsymbol{\nu}_i}) + \int_{(\partial\mathcal{D}^*_{\boldsymbol{\nu}_i})\cap K} (\Lambda\nabla\widehat{u}_h)\cdot\boldsymbol{n}\,\mathrm{d}s\right) = R_K(f, u_h, 1) = 0,$$

and complete the proof. □

Lemma 3 shows that, for each K, the local linear algebraic system (18) has linear correlation, and the coefficient matrix of (18) is $\mathbb{A}_K = (a_{ij})_{n\times n}$ with the entries

$$a_{ij} = -\int_{(\partial\mathcal{D}^*_{\boldsymbol{\nu}_i})\cap K} (\Lambda\nabla\psi_j)\cdot\boldsymbol{n}\,\mathrm{d}s, \quad i, j = 1, \cdots, n. \tag{20}$$

Thus, for the existence and uniqueness of $\widehat{u}_h$, it needs to satisfy (19) additionally. Here, we only analyze the one case, which consists in replacing the last equation in (18) with (19), and the other cases are similar. In this case, the new $n \times n$ local algebraic system is given by

$$\mathbb{B}_K \boldsymbol{c}_K = \boldsymbol{b}_K, \tag{21}$$

where $\boldsymbol{c}_K = (c_1, \cdots, c_n)^T$, and the entries of $\mathbb{B}_K$ and $\boldsymbol{b}_K$ are

$$b_{ij} = a_{ij}, \quad b_{n,j} = \frac{1}{81}, \quad i = 1, \cdots, n-1, \ j = 1, \cdots, n, \tag{22}$$

$$b_i = RHS_i, \quad b_n = 0, \quad i = 1, \cdots, n-1,$$

$$RHS_i = R_K(f, u_h, \phi_{\boldsymbol{\nu}_i}) + \int_{(\partial\mathcal{D}^*_{\boldsymbol{\nu}_i})\cap K} (\Lambda\nabla u_h)\cdot\boldsymbol{n}\,\mathrm{d}s. \tag{23}$$

If $\mathbb{B}_K$ is a nonsingular matrix, then we can obtain the existence and uniqueness of $\widehat{u}_h$. In brief, we summarize the above postprocessing technique in Algorithm 1.

Algorithm 1: The FVEM based on postprocessing technique.	
Step 1:	Compute the polygonal finite element solution u_h by (9);
Step 2:	Do $K \in \mathcal{M}$
	Solve the local linear algebraic system (21) on the cell K to get the coefficients c_j $(j = 1, \cdots, n)$ of (17);
	Enddo
Step 3:	Obtain the post-processed solution $\widehat{u}_h$ by (17).

4. Local conservation, existence and uniqueness

Theorem 1. *For the post-processed solution $\widehat{u}_h$ defined by* (17)-(19)*, it satisfies the following local conservation property*

$$-\int_{\partial \mathcal{D}^*_{\boldsymbol{\nu}}} (\Lambda \nabla \widehat{u}_h) \cdot \boldsymbol{n} \, \mathrm{d}s = \int_{\mathcal{D}^*_{\boldsymbol{\nu}}} f \, \mathrm{d}x\mathrm{d}y, \quad \forall \boldsymbol{\nu} \in \mathcal{V}^{int}. \tag{24}$$

Proof. Assume that $\omega_{\boldsymbol{\nu}} = \bigcup_i \{K_i : \boldsymbol{\nu} \in \overline{K}_i, \ K_i \in \mathcal{M}\}$, then for each $\boldsymbol{\nu} \in \mathcal{V}^{int}$, we deduce from (18), (16) and (9) that

$$\begin{aligned}
-\sum_{K \in \omega_{\boldsymbol{\nu}}} \int_{(\partial \mathcal{D}^*_{\boldsymbol{\nu}}) \cap K} (\Lambda \nabla \widehat{u}_h) \cdot \boldsymbol{n} \, \mathrm{d}s &= \sum_{K \in \omega_{\boldsymbol{\nu}}} R_K(f, u_h, \phi_{\boldsymbol{\nu}}) \\
&= \sum_{K \in \omega_{\boldsymbol{\nu}}} \left(\int_K f(\phi^*_{\boldsymbol{\nu}} - \phi_{\boldsymbol{\nu}}) \, \mathrm{d}x\mathrm{d}y + \int_K (\Lambda \nabla u_h) \cdot \nabla \phi_{\boldsymbol{\nu}} \, \mathrm{d}x\mathrm{d}y \right) \\
&= \int_{\mathcal{D}^*_{\boldsymbol{\nu}}} f \, \mathrm{d}x\mathrm{d}y + [a(u_h, \phi_{\boldsymbol{\nu}}) - (f, \phi_{\boldsymbol{\nu}})] \\
&= \int_{\mathcal{D}^*_{\boldsymbol{\nu}}} f \, \mathrm{d}x\mathrm{d}y.
\end{aligned}$$

Noticing

$$-\int_{\partial \mathcal{D}^*_{\boldsymbol{\nu}}} (\Lambda \nabla \widehat{u}_h) \cdot \boldsymbol{n} \, \mathrm{d}s = -\sum_{K \in \omega_{\boldsymbol{\nu}}} \int_{(\partial \mathcal{D}^*_{\boldsymbol{\nu}}) \cap K} (\Lambda \nabla \widehat{u}_h) \cdot \boldsymbol{n} \, \mathrm{d}s,$$

and then the desired result (24) is verified. □

Lemma 4. *Assume that the diffusion tensor Λ is constant on K. Then, for any $\boldsymbol{x}_K \in K$, we have*

$$a_{ii} = \frac{1}{96 A_i(\boldsymbol{x}_K)} \left(\boldsymbol{x}_i - \boldsymbol{x}_K\right)^T \mathcal{R}^T \Lambda \mathcal{R} \left(\boldsymbol{x}_i - \boldsymbol{x}_K\right), \quad i = 1, \cdots, n, \tag{25}$$

where $\boldsymbol{x}_i$ is the midpoint of line segment $\boldsymbol{\nu}_i \boldsymbol{\nu}_{i+1}$, see Figure 2, and $A_i(\boldsymbol{x})$ is defined by (4)*. Furthermore, under the assumption* (3)*, we have*

$$a_{ii} > 0, \quad i = 1, \cdots, n. \tag{26}$$

Proof. From (20) and (15), we have

$$a_{ii} = -\int_{\boldsymbol{x}_i \boldsymbol{x}_K} (\Lambda \nabla \psi_i) \cdot \boldsymbol{n} \, \mathrm{d}s, \tag{27}$$

where $\boldsymbol{n} = -\mathcal{R} \left(\boldsymbol{x}_i - \boldsymbol{x}_K\right) / |\boldsymbol{x}_i \boldsymbol{x}_K|$. By direct calculations,

$$\nabla \psi_i(\boldsymbol{x}_K) + 4 \nabla \psi_i \left(\frac{\boldsymbol{x}_K + \boldsymbol{x}_i}{2} \right) + \nabla \psi_i(\boldsymbol{x}_i) = \frac{1}{16 A_i(\boldsymbol{x}_K)} \mathcal{R} \left(\boldsymbol{x}_i - \boldsymbol{x}_K\right).$$

Since the integrand of (27) is a cubic function, by the Simpson's rule, one reaches (25). Recalling that $A_i(\boldsymbol{x}_K) > 0$ and $\boldsymbol{x}_i \neq \boldsymbol{x}_K$, then (26) is a direct consequence of (3) and (25). $\square$

Theorem 2. *Suppose that the diffusion tensor Λ is constant on any cell in $\mathcal{M}$. Then, there exists a unique $\widehat{u}_h$, satisfying* (17), (18) *and* (19) *simultaneously.*

Proof. What we need is to prove that the matrix $\mathbb{B}_K$ in (21) is nonsingular. Let $a_{n+1,n} = a_{1,n}$. Then, from (20) and (15), we have

$$a_{ii} + a_{i+1,i} = 0, \quad i = 1, \cdots, n \tag{28}$$

and

$$a_{ij} = 0, \quad j \neq i-1, i. \tag{29}$$

It follows from (22) that

$$\begin{aligned}
\det(\mathbb{B}_K) &= \frac{1}{81}\begin{vmatrix}
a_{11} & 0 & 0 & \cdots & 0 & 0 & -a_{n,n} \\
a_{21} & a_{22} & 0 & \cdots & 0 & 0 & 0 \\
0 & a_{32} & a_{33} & \cdots & 0 & 0 & 0 \\
\vdots & \vdots & \vdots & & \vdots & \vdots & \vdots \\
0 & 0 & 0 & \cdots & a_{n-2,n-2} & 0 & 0 \\
0 & 0 & 0 & \cdots & a_{n-1,n-2} & a_{n-1,n-1} & 0 \\
1 & 1 & 1 & \cdots & 1 & 1 & 1
\end{vmatrix} \\
&= \frac{1}{81}\begin{vmatrix}
a_{11} & 0 & 0 & \cdots & 0 & 0 & -a_{n,n} \\
0 & a_{22} & 0 & \cdots & 0 & 0 & -a_{n,n} \\
0 & 0 & a_{33} & \cdots & 0 & 0 & -a_{n,n} \\
\vdots & \vdots & \vdots & & \vdots & \vdots & \vdots \\
0 & 0 & 0 & \cdots & a_{n-2,n-2} & 0 & -a_{n,n} \\
0 & 0 & 0 & \cdots & 0 & a_{n-1,n-1} & -a_{n,n} \\
1 & 1 & 1 & \cdots & 1 & 1 & 1
\end{vmatrix} \\
&= \frac{1}{81}\prod_{i=1}^{n} a_{ii} \sum_{i=1}^{n} \frac{1}{a_{ii}},
\end{aligned} \tag{30}$$

which implies the nonsingularity of $\mathbb{B}_K$ and verifies the result of this theorem by Lemma 4. $\square$

5. Error estimates

To begin with, we introduce the following geometric assumption.

- (**G6**) There exists a positive constant r_*, independent of h, such that
$$d_{K,i} > r_* h_K, \quad i = 1, \cdots, n, \quad \forall\, K \in \mathcal{M},$$
where $d_{K,i}$ denotes the distance from the cell center $\boldsymbol{x}_K$ to the edge $\boldsymbol{\nu}_i\boldsymbol{\nu}_{i+1}$.

Proposition 4. *Under the geometric assumption* (**G1**)*, there exists at least one point $\boldsymbol{x}_K \in K$ satisfying the geometric assumption* (**G6**).

Proof. For example, let $\boldsymbol{x}_K$ be the center of the largest circle inscribed in K. From (**G1**), we find that

$$d_{K,i} \geq \rho_K > \frac{1}{\gamma^*} h_K,$$

which leads to (**G6**) with $r_* = 1/\gamma^*$. The proof is complete. $\square$

Lemma 5. *Suppose that the diffusion tensor* Λ *is piecewise constant with respect to the primary mesh, or alternatively, piecewise* $W^{1,\infty}$ *and the mesh size* h *is small enough. Then, under the assumptions* (3), (**G2**) *and* (**G6**), *we have*

$$\det(\mathbb{B}_K) \sim 1, \quad \forall\, K \in \mathcal{M}. \tag{31}$$

Proof. Firstly, we prove the case when Λ is piecewise constant with respect to the primary mesh. From (**G2**) and (**G6**), we have

$$\frac{1}{2} h_K^2 > A_i(\boldsymbol{x}_K) = \frac{1}{2} d_{K,i} \|\boldsymbol{\nu}_i - \boldsymbol{\nu}_{i+1}\| > \frac{1}{2} r_* d_* h_K^2,$$

$$h_K > \|\boldsymbol{x}_i - \boldsymbol{x}_K\| \geq d_{K,i} > r_* h_K.$$

It follows from (25) and (3) that

$$\frac{\underline{\lambda} r_*^2}{48} < \frac{\underline{\lambda} \|\boldsymbol{x}_i - \boldsymbol{x}_K\|^2}{96 A_i(\boldsymbol{x}_K)} \leq a_{ii} \leq \frac{\overline{\lambda} \|\boldsymbol{x}_i - \boldsymbol{x}_K\|^2}{96 A_i(\boldsymbol{x}_K)} < \frac{\overline{\lambda}}{48 r_* d_*}, \quad i = 1, \cdots, n.$$

Recall that (**G2**) implies (**G5**). Hence, combining the above estimate with (30) leads to (31).

Secondly, we consider the general case where Λ is piecewise $W^{1,\infty}$ with respect to the primary mesh. Let

$$\overline{\Lambda}|_K = \Lambda(\boldsymbol{x}_K), \quad \forall\, K \in \mathcal{M}.$$

By replacing Λ with $\overline{\Lambda}$ in (20), we get the matrix $\overline{\mathbb{B}}_K = (\bar{b}_{ij})_{n \times n}$ in a way similar to that of $\mathbb{B}_K$. Similar to the above arguments, we find that (31) also holds for $\overline{\mathbb{B}}_K$. According to (15), we know $\|\nabla \psi_j\| \lesssim h_K^{-1}, \forall \boldsymbol{x} \in (\partial \mathcal{D}^*_{\boldsymbol{\nu}_i}) \cap K$, where we have used the facts that in $\triangle \boldsymbol{x}_K \boldsymbol{\nu}_j \boldsymbol{\nu}_{j+1}$

$$|\lambda_{\boldsymbol{\nu}}| \lesssim 1, \quad \|\nabla \lambda_{\boldsymbol{\nu}}\| \lesssim h_K^{-1},$$

and $\lambda_{\boldsymbol{\nu}}$ is any linear nodal basis function. Then we have $|b_{ij} - \bar{b}_{ij}| \lesssim h$ and

$$\left|\det(\mathbb{B}_K) - \det\left(\overline{\mathbb{B}}_K\right)\right| \lesssim h.$$

Therefore, when the mesh size h is sufficiently small, one can still reach (31). The proof is complete. $\square$

Lemma 6. *Under the assumptions* (**G2**) *and* (**G3**), *for any* $K \in \mathcal{M}$ *with* $h_K = 1$, *we have*

$$\|u_h\|_{0,K} \sim \|u_h\|_{0,K,h}, \quad \forall\, u_h \in U_h, \tag{32}$$

where the discrete norm

$$\|u_h\|_{0,K,h}^2 = \sum_{i=1}^{n} u_i^2, \quad u_i = u_h(\boldsymbol{\nu}_i).$$

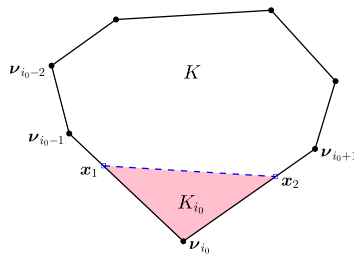

FIGURE 4. A triangle K_{i_0} used in the proof of Lemma 6.

Proof. On the one hand, we have

$$\|u_h\|_{0,K} \leq \sum_{i=1}^{n} |u_i| \|\phi_i\|_{0,K} < \sum_{i=1}^{n} |u_i| \leq \sqrt{n^*} \left(\sum_{i=1}^{n} u_i^2 \right)^{\frac{1}{2}} \lesssim \|u_h\|_{0,K,h}.$$

On the other hand, we denote $|u_{i_0}| = \max_{1 \leq i \leq n} |u_i|$, and we first consider the case $n \geq 4$. Set $d_* = \min\{d_*, 1/2\}$ and

$$r_0 = \frac{d_*^{4n^*-4} \beta^{2n^*-2}}{2n^*} < \frac{1}{10}, \quad \beta = \min\{\sin \alpha^*, \sin \alpha_*\}.$$

We define two points $\boldsymbol{x}_1$ and $\boldsymbol{x}_2$ which belong to the line segments $\boldsymbol{\nu}_{i_0}\boldsymbol{\nu}_{i_0-1}$ and $\boldsymbol{\nu}_{i_0}\boldsymbol{\nu}_{i_0+1}$ (see Figure 4), satisfying

$$\frac{|\boldsymbol{\nu}_{i_0}\boldsymbol{x}_1|}{|\boldsymbol{\nu}_{i_0}\boldsymbol{\nu}_{i_0-1}|} = \frac{|\boldsymbol{\nu}_{i_0}\boldsymbol{x}_2|}{|\boldsymbol{\nu}_{i_0}\boldsymbol{\nu}_{i_0+1}|} = r_0,$$

and denote $K_{i_0} := \triangle \boldsymbol{x}_1 \boldsymbol{\nu}_{i_0} \boldsymbol{x}_2$. By Lemma 2 of [42], we have

$$A_i(\boldsymbol{\nu}_j) \geq \frac{1}{2} d_*^4 \beta^2, \quad \forall\, j \neq i, i+1.$$

As a result, for any $i \notin \{i_0 - 2, i_0 - 1, i_0, i_0 + 1\}$

$$A_i(\boldsymbol{x}) \geq \min\{A_i(\boldsymbol{\nu}_{i_0-1}), A_i(\boldsymbol{\nu}_{i_0}), A_i(\boldsymbol{\nu}_{i_0+1})\} \geq \frac{1}{2} d_*^4 \beta^2, \quad \forall\, \boldsymbol{x} \in K_{i_0}.$$

Moreover,

$$\begin{aligned} A_{i_0-2}(\boldsymbol{x}) &\geq \min\{A_{i_0-2}(\boldsymbol{x}_1), A_{i_0-2}(\boldsymbol{\nu}_{i_0}), A_{i_0-2}(\boldsymbol{\nu}_{i_0+1})\} \\ &\geq \min\left\{ \frac{1}{2} d_*^2 \beta (1 - r_0),\ \frac{1}{2} d_*^4 \beta^2 \right\} = \frac{1}{2} d_*^4 \beta^2, \quad \forall\, \boldsymbol{x} \in K_{i_0}, \end{aligned}$$

where the fact $1 - r_0 > d_*^2 \beta$ is used. Similarly, we have $A_{i_0+1}(\boldsymbol{x}) \geq d_*^4 \beta^2 / 2$, $\forall\, \boldsymbol{x} \in K_{i_0}$, and

$$\max\{A_{i_0-1}(\boldsymbol{x}), A_{i_0}(\boldsymbol{x})\} \leq \frac{1}{2} r_0, \quad \forall\, \boldsymbol{x} \in K_{i_0}.$$

Then, for any $\boldsymbol{x} \in K_{i_0}$, we have

$$w_i(\boldsymbol{x}) \begin{cases} \geq \dfrac{1}{2^{n-1}} d_*^{4n-4} \beta^{2n-2}, & i = i_0, \\ \leq \dfrac{r_0}{2^{n-1}}, & i = i_0 - 1, i_0 + 1, \\ \leq \dfrac{r_0^2}{2^{n-1}} < \dfrac{r_0}{2^{n-1}}, & i \neq i_0 - 1, i_0, i_0 + 1. \end{cases}$$

It follows that

$$\begin{aligned}\left|\sum_{i=1}^{n} u_i w_i(\boldsymbol{x})\right| \geq & |u_{i_0}| w_{i_0}(\boldsymbol{x}) - \sum_{1\leq i\leq n, i\neq i_0} |u_i| w_i(\boldsymbol{x}) \\ \geq & |u_{i_0}| \left(w_{i_0}(\boldsymbol{x}) - \sum_{1\leq i\leq n, i\neq i_0} w_i(\boldsymbol{x}) \right) \\ \geq & \frac{1}{2^{n^*}}\ d_*^{4n^*-4}\beta^{2n^*-2}|u_{i_0}|, \quad \forall\, \boldsymbol{x}\in K_{i_0}.\end{aligned}$$

Due to $\sum_{i=1}^{n} w_i(\boldsymbol{x}) < n/2^{n-1} \leq 1/2,\ \forall\, \boldsymbol{x}\in K$, we have

$$\begin{aligned}\|u_h\|_{0,K} \geq & \|u_h\|_{0,K_{i_0}} \geq 2\left\|\sum_{i=1}^{n} u_i w_i(\boldsymbol{x})\right\|_{0,K_{i_0}} \geq \frac{d_*^{4n^*-4}\beta^{2n^*-2}}{2^{n^*-1}}|u_{i_0}||K_{i_0}|^{\frac{1}{2}} \\ \geq & \frac{d_*^{8n^*-7}\beta^{4n^*-7/2}}{2^{n^*+1/2}n^*}|u_{i_0}| \geq \frac{d_*^{8n^*-7}\beta^{4n^*-7/2}}{2^{n^*+1/2}\,(n^*)^{3/2}}\|u_h\|_{0,K,h},\end{aligned}$$

where $|K_{i_0}|$ denotes the area of K_{i_0}. For the case $n = 3$, the Wachspress shape functions reduce to the classical linear nodal basis functions, and the proof of above inequality is trivial. Thus, we reach (32) for any $n \geq 3$. □

Lemma 7. *Under the assumptions* (**G2**) *and* (**G3**)*, for any $K \in \mathcal{M}$, we have*

$$|u_h|_{2,K} \lesssim h_K^{-1}|u_h|_{1,K}, \quad \forall\, u_h \in U_h. \tag{33}$$

Proof. By the following scaling transformation

$$\mathcal{J}_K(\boldsymbol{x}) := \widehat{\boldsymbol{x}} = \frac{\boldsymbol{x}-\boldsymbol{x}_K}{h_K},$$

we can map the cell K to $\widehat{K}$ with $h_{\widehat{K}} = 1$. According to the facts $|\phi_i|_{1,K} \lesssim 1$ (see Lemma 6 of [13]) and $|\phi_i|_{2,K} \lesssim h_K^{-1}$ (see Lemma 4 of [42]), we deduce that

$$\|u_h\|_{2,\widehat{K}} \leq \sum_{i=1}^{n} |u_i|\|\phi_i\|_{2,\widehat{K}} \lesssim \sum_{i=1}^{n}|u_i| \lesssim \|u_h\|_{0,\widehat{K},h} \lesssim \|u_h\|_{0,\widehat{K}},$$

where we have used the fact (32) in the last inequality. Let

$$\bar{u}_h = \frac{1}{|\widehat{K}|}\int_{\widehat{K}} u_h\,\mathrm{d}x\mathrm{d}y,$$

it follows that

$$|u_h|_{2,\widehat{K}} = |u_h - \bar{u}_h|_{2,\widehat{K}} \leq \|u_h-\bar{u}_h\|_{2,\widehat{K}} \lesssim \|u_h-\bar{u}_h\|_{0,\widehat{K}} \lesssim |u_h|_{1,\widehat{K}},$$

where in the last inequality we used the fact (1.11) of [2]. Finally, we obtain

$$|u_h|_{2,K} = h_K^{-1}|u_h|_{2,\widehat{K}} \lesssim h_K^{-1}|u_h|_{1,\widehat{K}} = h_K^{-1}|u_h|_{1,K},$$

and complete the proof. □

Theorem 3. *Suppose that $\mathcal{T}_h$ is an arbitrary convex polygonal mesh. Let Λ be subjected to the same assumptions in Lemma 5, and u be the exact solution of* (1) *and* (2)*. Then, under the assumptions* (3), (**G2**), (**G3**) *and* (**G6**)*, for the post-processed solution $\widehat{u}_h$ defined by* (17)-(19)*, we have*

$$\|u-\widehat{u}_h\|_m \lesssim h^{2-m}\|u\|_2, \quad m=0,1. \tag{34}$$

Proof. By recalling (12), in order to prove (34), we only need to prove

$$\|\widehat{u}_h - u_h\|_m \lesssim h^{2-m}\|u\|_2, \quad m = 0, 1. \tag{35}$$

Note that in each $K \in \mathcal{M}$, we have

$$\widehat{u}_h - u_h = \sum_{j=1}^{n} c_j \psi_j.$$

Moreover, by (28), (29) and Lemma 5, there holds $|a_{ij}| \lesssim 1$, $i, j = 1, \cdots, n$. Then, from (21) and (31),

$$|c_j| \lesssim \max_{1\le i\le n} |RHS_i|, \quad j = 1, \cdots, n.$$

By (1) and the Green's formula, for any $i = 1, \cdots, n$, we have

$$\begin{aligned}\int_K f\phi^*_{\boldsymbol{\nu}_i}\,\mathrm{d}x\mathrm{d}y &= \int_{\mathcal{D}^*_{\boldsymbol{\nu}_i}\cap K} f\,\mathrm{d}x\mathrm{d}y = -\int_{\mathcal{D}^*_{\boldsymbol{\nu}_i}\cap K} \nabla\cdot(\Lambda\nabla u)\,\mathrm{d}x\mathrm{d}y \\ &= -\int_{\partial(\mathcal{D}^*_{\boldsymbol{\nu}_i}\cap K)} (\Lambda\nabla u)\cdot\boldsymbol{n}\,\mathrm{d}s\end{aligned}$$

and

$$\begin{aligned}\int_K f\phi_{\boldsymbol{\nu}_i}\,\mathrm{d}x\mathrm{d}y &= -\int_K \nabla\cdot(\Lambda\nabla u)\phi_{\boldsymbol{\nu}_i}\,\mathrm{d}x\mathrm{d}y \\ &= \int_K (\Lambda\nabla u)\cdot\nabla\phi_{\boldsymbol{\nu}_i}\,\mathrm{d}x\mathrm{d}y - \int_{\partial K}(\Lambda\nabla u)\cdot\boldsymbol{n}\phi_{\boldsymbol{\nu}_i}\,\mathrm{d}s.\end{aligned}$$

According to (16) and (23),

$$\begin{aligned}RHS_i &= \int_K f(\phi^*_{\boldsymbol{\nu}_i} - \phi_{\boldsymbol{\nu}_i})\,\mathrm{d}x\mathrm{d}y + \int_K (\Lambda\nabla u_h)\cdot\nabla\phi_{\boldsymbol{\nu}_i}\,\mathrm{d}x\mathrm{d}y \\ &\quad + \int_{\partial K}\{\Lambda\nabla u_h\}\cdot\boldsymbol{n}(\phi^*_{\boldsymbol{\nu}_i} - \phi_{\boldsymbol{\nu}_i})\,\mathrm{d}s + \int_{(\partial\mathcal{D}^*_{\boldsymbol{\nu}_i})\cap K}(\Lambda\nabla u_h)\cdot\boldsymbol{n}\,\mathrm{d}s \\ &= E_1 + E_2 + E_3 + E_4,\end{aligned}$$

where

$$E_1 = \int_K (\Lambda\nabla(u_h - u))\cdot\nabla\phi_{\boldsymbol{\nu}_i}\,\mathrm{d}x\mathrm{d}y, \qquad E_2 = \int_{(\partial\mathcal{D}^*_{\boldsymbol{\nu}_i})\cap K}(\Lambda\nabla(u_h - u))\cdot\boldsymbol{n}\,\mathrm{d}s,$$

$$E_3 = \int_{\mathcal{D}^*_{\boldsymbol{\nu}_i}\cap\partial K}(\{\Lambda\nabla u_h\} - \Lambda\nabla u)\cdot\boldsymbol{n}\,\mathrm{d}s, \quad E_4 = \int_{\partial K}(\Lambda\nabla u - \{\Lambda\nabla u_h\})\cdot\boldsymbol{n}\phi_{\boldsymbol{\nu}_i}\,\mathrm{d}s.$$

It follows from the Cauchy-Schwartz inequality and trace inequality that

$$|E_1| \lesssim |u - u_h|_{1,K}|\phi_{\boldsymbol{\nu}_i}|_{1,K} \lesssim |u - u_h|_{1,K}, \quad |E_2| \lesssim |u - u_h|_{1,K} + h_K|u - u_h|_{2,K},$$

where we have used the fact $|\phi_{\boldsymbol{\nu}_i}|_{1,K} \lesssim 1$ (see Lemma 2 of [13]). By the same arguments,

$$|E_3| + |E_4| \lesssim \int_{\partial K}|\{\Lambda\nabla u_h\} - \Lambda\nabla u|\,\mathrm{d}s \lesssim |u - u_h|_{1,\omega_K} + h_K|u - u_h|_{2,\omega_K},$$

where $\omega_K = \{K\}\cup\{L : L \text{ and } K \text{ have one common edge}\}$. Therefore,

$$|RHS_i| \lesssim |u - u_h|_{1,\omega_K} + h_K|u - u_h|_{2,\omega_K}, \quad i = 1, \cdots, n.$$

From the triangle inequality, (11) and (33)

$$\begin{aligned}|u - u_h|_{2,K} &< |u - u_I|_{2,K} + |u_I - u_h|_{2,K} \lesssim |u|_{2,K} + h_K^{-1}|u_I - u_h|_{1,K} \\ &\lesssim |u|_{2,K} + h_K^{-1}|u - u_h|_{1,K}.\end{aligned}$$

By recalling (15), the bubble function ψ_j is a polynomial in $\triangle \boldsymbol{x}_K \boldsymbol{\nu}_i \boldsymbol{\nu}_{i+1}$ and vanishes outside of this triangle, then we have

$$\|\psi_j\|_{m,K} \lesssim h_K^{1-m}, \quad m = 0, 1.$$

It follows that

$$\begin{aligned}\|\widehat{u}_h - u_h\|_{m,K} &\leq \sum_{j=1}^{n} |c_j| \|\psi_j\|_{m,K} \lesssim h_K^{1-m} \max_{1\leq j\leq n} |c_j| \lesssim h_K^{1-m} \max_{1\leq i\leq n} |RHS_i| \\ &\lesssim h_K^{1-m} |u - u_h|_{1,\omega_K} + h_K^{2-m} \|u\|_{2,\omega_K}, \quad m = 0, 1.\end{aligned}$$

Note that (12), then (35) is obtained by summing up the above inequality over all polygonal cells. The proof is complete. □

Remark 1. *We mention that in our numerical analysis, some bubble functions cannot be chosen. For instance, in Lemma 4, if* $\psi_i = \lambda_{\boldsymbol{x}_K}^m \lambda_{\boldsymbol{\nu}_i} \lambda_{\boldsymbol{\nu}_{i+1}}$ $(m \geq 1)$*, then we find that* $a_{ii} = 0$*. In other words, we cannot choose* $\lambda_{\boldsymbol{x}_K}^m \lambda_{\boldsymbol{\nu}_j} \lambda_{\boldsymbol{\nu}_{j+1}}$ *in* (15)*. However, similar to the previous discussions, instead of* (15)*, one can choose* $\psi_j = \lambda_{\boldsymbol{x}_K} \lambda_{\boldsymbol{\nu}_j} \lambda_{\boldsymbol{\nu}_{j+1}}^2$*. For this special case (i.e.* $a_{ii} < 0$*), the existence, uniqueness and optimal error estimates of the new polygonal finite volume element solution can be verified by the same arguments.*

6. Numerical experiments

In this section, we present two numerical examples to verify the theoretical findings, where the first (resp. second) one is designed for continuous (resp. discontinuous) diffusion tensor. In our numerical experiments, we choose the square domain $\Omega = [0, 1]^2$, and employ four types of meshes, see Figures 5-8. Moreover, the following L^2 error E_u, H^1 error E_q and local conservation error E_c are used to measure the errors of new polygonal finite volume element solution $\widehat{u}_h$

$$\begin{aligned}&E_u = \|u - \widehat{u}_h\|_0, \quad E_q = \|\nabla(u - \widehat{u}_h)\|_0, \\ &E_c(\widehat{u}_h) = \max_{\boldsymbol{\nu}\in\mathcal{V}^{int}} \left| \int_{\partial\mathcal{D}_{\boldsymbol{\nu}}^*} (\Lambda\nabla\widehat{u}_h) \cdot \boldsymbol{n} \, \mathrm{d}s + \int_{\mathcal{D}_{\boldsymbol{\nu}}^*} f \, \mathrm{d}x\mathrm{d}y \right|.\end{aligned}$$

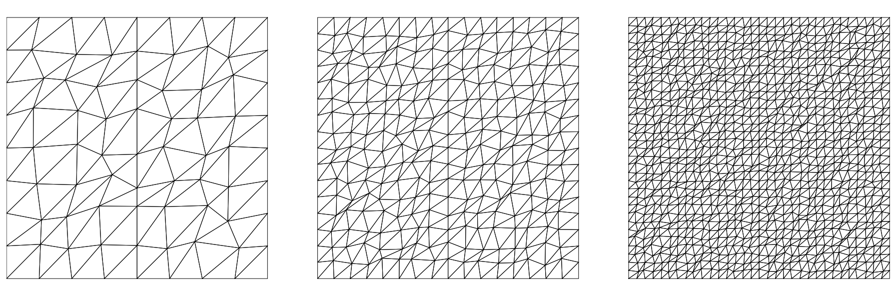

(a) level 1 (b) level 2 (c) level 3

FIGURE 5. Mesh 1: Triangular mesh.

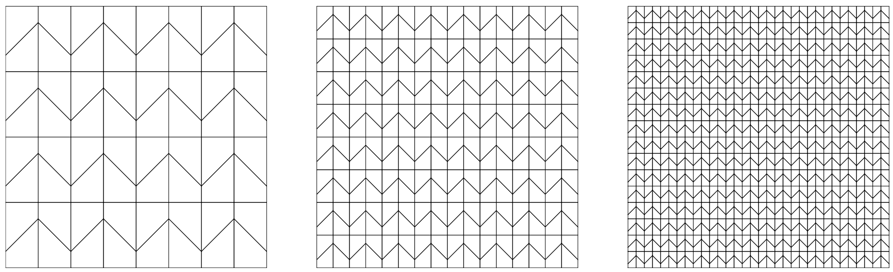

(a) level 1 (b) level 2 (c) level 3

FIGURE 6. Mesh 2: Trapezoidal mesh.

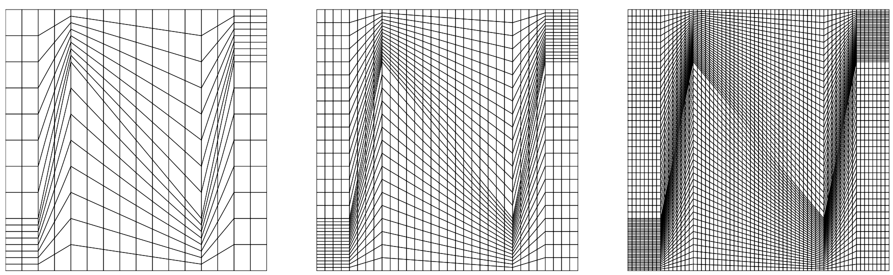

(a) level 1 (b) level 2 (c) level 3

FIGURE 7. Mesh 3: Kershaw mesh.

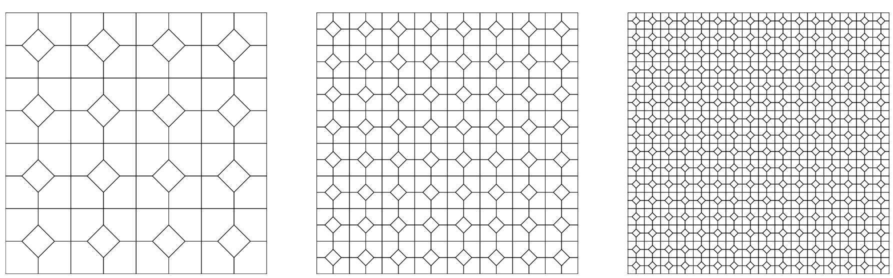

(a) level 1 (b) level 2 (c) level 3

FIGURE 8. Mesh 4: Polygonal mesh.

6.1. Example 1. We consider the anisotropic diffusion equation with the diffusion tensor and exact solution as follows

$$\Lambda = \begin{pmatrix} 1.0 & 0.2 \\ 0.2 & 0.5 \end{pmatrix}, \quad u(x, y) = e^{0.1x+0.2y},$$

where the source term and Dirichlet boundary condition are chosen to match the exact solution. Table 1 shows the H^1 and L^2 errors of the new finite volume element solution $\widehat{u}_h$ on polygonal meshes, the convergence orders are 1 and 2 respectively, which validates the theoretical results in Theorem 3. More importantly, the local conservation errors for the finite element (FE) solution (blue lines, $E_c(u_h)$) and new finite volume element (FVE) solution (red lines, $E_c(\widehat{u}_h)$) are plotted in Figure 9,

TABLE 1. The numerical results for Example 1.

Mesh		level 1	level 2	level 3	level 4	level 5
Mesh 1	h	2.44350E-01	1.19675E-01	6.18235E-02	3.15954E-02	1.60541E-02
	E_q	3.32576E-03	1.64382E-03	8.15878E-04	4.09471E-04	2.05044E-04
	Order		0.98719	1.06059	1.02700	1.02156
	E_u	1.36503E-04	3.35805E-05	8.34939E-06	2.11693E-06	5.30697E-07
	Order		1.96463	2.10715	2.04421	2.04348
Mesh 2	h	2.25347E-01	1.12673E-01	5.63367E-02	2.81684E-02	1.40842E-02
	E_q	3.05035E-03	1.52185E-03	7.60082E-04	3.79831E-04	1.89863E-04
	Order		1.00314	1.00160	1.00080	1.00040
	E_u	1.61203E-04	4.03736E-05	1.01036E-05	2.52733E-06	6.32023E-07
	Order		1.99739	1.99854	1.99919	1.99956
Mesh 3	h	3.67848E-01	1.93169E-01	9.88984E-02	5.00278E-02	2.51586E-02
	E_q	7.83261E-03	4.03550E-03	1.72881E-03	7.75492E-04	3.71155E-04
	Order		1.02960	1.26621	1.17634	1.07201
	E_u	3.70236E-04	1.19882E-04	3.27233E-05	8.38704E-06	2.11161E-06
	Order		1.75071	1.93945	1.99762	2.00652
Mesh 4	h	1.76777E-01	8.83883E-02	4.41942E-02	2.20971E-02	1.10485E-02
	E_q	1.75218E-03	8.76234E-04	4.38164E-04	2.19095E-04	1.09551E-04
	Order		0.99976	0.99985	0.99991	0.99995
	E_u	7.98227E-05	1.99335E-05	4.98168E-06	1.24530E-06	3.11317E-07
	Order		2.00160	2.00049	2.00014	2.00003

and the latter one is almost machine precision. In other words, the post-processed solution satisfies the local conservation law on the dual mesh, which confirms the findings in Theorem 1.

6.2. Example 2. In this example, the discontinuous diffusion tensor and exact solution are given by

$$\Lambda = \begin{cases} \Lambda_1, & x \le 0.5, \\ \Lambda_2, & x > 0.5, \end{cases} \qquad \Lambda_1 = \begin{pmatrix} 1 & 0 \\ 0 & 1 \end{pmatrix}, \quad \Lambda_2 = \begin{pmatrix} 10 & 3 \\ 3 & 1 \end{pmatrix},$$

$$u(x,y) = \begin{cases} -2y^2 + 4xy + 6x + 2y + 1, & x \le 0.5, \\ -2y^2 + 1.6xy - 0.6x + 3.2y + 4.3, & x > 0.5. \end{cases}$$

The numerical results are given in Table 2, one can observe that the performance is similar to the previous example.

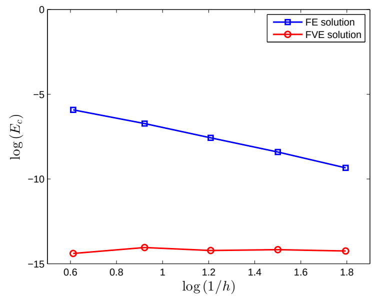

(a) Mesh 1

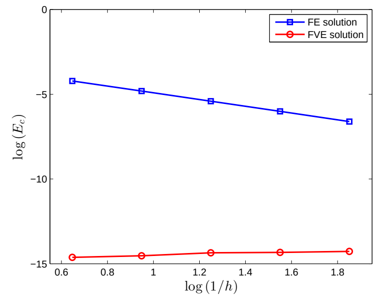

(b) Mesh 2

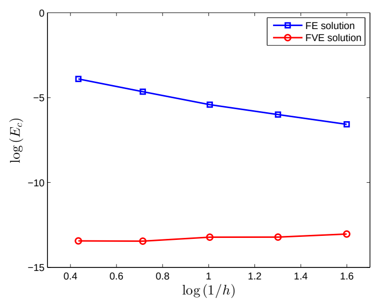

(c) Mesh 3

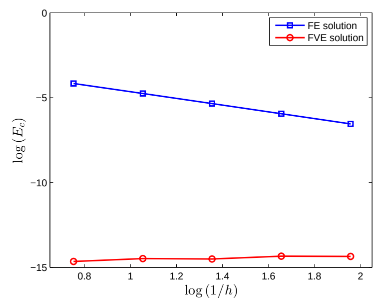

(d) Mesh 4

FIGURE 9. The local conservation errors for FE and new FVE solutions for Example 1.

7. Conclusions

In this article, we provided a new finite volume element solution for solving the anisotropic diffusion problem on arbitrary convex polygonal meshes. The new solution is obtained by postprocessing the finite element solution of the prescribed diffusion equation, where the shape function of finite element space is constructed by Wachspress generalized barycentric coordinate. Precisely, by adding some special designed element-wise bubble functions to the finite element solution, the existence and uniqueness of the new solution are verified on arbitrary convex polygonal meshes. Moreover, we proved that the new finite volume element solution satisfies the local conservation property on a certain dual mesh, and preserves the optimal H^1 and L^2 error estimates on the primary mesh.

Acknowledgments

The authors thank the reviewers for the carefully readings and providing some insightful comments and suggestions. This work was partially supported by the Guangdong Basic and Applied Basic Research Foundation (Nos. 2022A1515012106, 2023A1515010885), the project of Guangdong Polytechnic Normal University (No. 2022SDKYA023) and the scientific research capacity improvement project of the doctoral program construction unit of Guangdong Polytechnic Normal University in 2022 (No. 22GPNUZDJS31).

TABLE 2. The numerical results for Example 2.

Mesh		level 1	level 2	level 3	level 4	level 5
Mesh 1	h	2.44350E-01	1.19675E-01	6.18235E-02	3.15954E-02	1.60541E-02
	E_q	2.14845E-01	1.12647E-01	5.59826E-02	2.80591E-02	1.40465E-02
	Order		0.90451	1.05863	1.02898	1.02200
	E_u	4.75347E-03	1.31272E-03	3.49202E-04	8.79593E-05	2.24836E-05
	Order		1.80265	2.00487	2.05398	2.01476
	$E_c(\widehat{u}_h)$	1.87E-013	1.74E-013	2.09E-013	2.30E-013	2.19E-013
Mesh 2	h	2.25347E-01	1.12673E-01	5.63367E-02	2.81684E-02	1.40842E-02
	E_q	3.06026E-01	1.53441E-01	7.67431E-02	3.83648E-02	1.91790E-02
	Order		0.99597	0.99958	1.00025	1.00026
	E_u	1.24795E-02	3.08162E-03	7.66048E-04	1.91018E-04	4.76960E-05
	Order		2.01780	2.00818	2.00373	2.00177
	$E_c(\widehat{u}_h)$	1.21E-013	1.53E-013	1.94E-013	1.95E-013	1.92E-013
Mesh 3	h	3.67848E-01	1.93169E-01	9.88984E-02	5.00278E-02	2.51586E-02
	E_q	6.80312E-01	2.82764E-01	1.11747E-01	4.56999E-02	2.04676E-02
	Order		1.36304	1.38672	1.31200	1.16857
	E_u	2.59377E-02	1.01941E-02	3.21009E-03	8.90422E-04	2.35789E-04
	Order		1.44990	1.72600	1.88163	1.93308
	$E_c(\widehat{u}_h)$	1.11E-012	1.86E-012	4.53E-012	2.67E-012	3.25E-012
Mesh 4	h	1.76777E-01	8.83883E-02	4.41942E-02	2.20971E-02	1.10485E-02
	E_q	1.73084E-01	8.68707E-02	4.35224E-02	2.17833E-02	1.08973E-02
	Order		0.99453	0.99711	0.99853	0.99926
	E_u	6.10702E-03	1.52119E-03	3.79721E-04	9.48717E-05	2.37115E-05
	Order		2.00527	2.00219	2.00089	2.00039
	$E_c(\widehat{u}_h)$	5.02E-014	1.04E-013	1.46E-013	1.58E-013	2.08E-013

References

[1] R. E. Bank and D. J. Rose, Some error estimates for the box method, SIAM J. Numer. Anal., 24: 777-787, 1987.
[2] D. Braess, Finite elements: theory, fast solvers, and applications in solid mechanics, 3rd ed. Cambridge University Press, New York, 2007.
[3] S. C. Brenner and L. R. Scott, The mathematical theory of finite element methods, 3rd ed. Springer-Verlag, New York, 2008.

[4] L. Bush and V. Ginting, On the application of the continuous Galerkin finite element method for conservation problems, SIAM J. Sci. Comput., 35: A2953-A2975, 2013.
[5] Z. Cai, On the finite volume element method, Numer. Math., 58: 713-735, 1991.
[6] Z. Chen, J. Wu and Y. Xu, Higher-order finite volume methods for elliptic boundary value problems, Adv. Comput. Math., 37: 191-253, 2012.
[7] S. Chou and X. Ye, Unified analysis of finite volume methods for second order elliptic problems, SIAM J. Numer. Anal., 45: 1639-1653, 2007.
[8] B. Cockburn, J. Gopalakrishnan and H. Wang, Locally conservative fluxes for the continuous Galerkin method, SIAM J. Numer. Anal., 45: 1742-1776, 2007.
[9] R. E. Ewing, T. Lin and Y. Lin, On the accuracy of the finite volume element method based on piecewise linear polynomials, SIAM J. Numer. Anal., 39: 1865-1888, 2002.
[10] M. Floater, Mean value coordinates, Comput. Aided Geom. Des., 20: 19-27, 2003.
[11] M. Floater, Generalized barycentric coordinates and applications, Acta Numer., 24: 161-214, 2015.
[12] M. Floater, K. Hormann and G. Kós, A general construction of barycentric coordinates over convex polygons, Adv. Comput. Math., 24: 311-331, 2006.
[13] A. Gillette, A. Rand and C. Bajaj, Error estimates for generalized barycentric interpolation, Adv. Comput. Math., 37: 417-439, 2012.
[14] W. He, Z. Zhang and Q. Zou, Maximum-norms error estimates for high-order finite volume schemes over quadrilateral meshes, Numer. Math., 138: 473-500, 2018.
[15] Q. Hong and J. Wu, A Q_1-finite volume element scheme for anisotropic diffusion problems on general convex quadrilateral mesh, J. Comput. Appl. Math., 372: 112732, 2020.
[16] K. Hormann and N. Sukumar, Generalized barycentric coordinates in computer graphics and computational mechanics, CRC press, Boca Raton, 2017.
[17] S. Lee, Y. Lee and M. Wheeler, A locally conservative enriched Galerkin approximation and efficient solver for elliptic and parabolic problems, SIAM J. Sci. Comput., 38: A1404-A1429, 2016.
[18] R. Li, Z. Chen and W. Wu, Generalized difference methods for differential equations: Numerical analysis of finite volume methods, Marcel Dekker, New York, 2000.
[19] Y. Li and R. Li, Generalized difference methods on arbitrary quadrilateral networks, J. Comput. Math., 17: 653-672, 1999.
[20] Y. Lin, J. Liu and M. Yang, Finite volume element methods: an overview on recent developments, Int. J. Numer. Anal. Mod., B 4: 14-34, 2013.
[21] Y. Lin, M. Yang and Q. Zou, L^2 error estimates for a class of any order finite volume schemes over quadrilateral meshes, SIAM J. Numer. Anal., 53: 2030-2050, 2015.
[22] Y. Liu, Y. Feng and R. Zhang, A high order conservative flux optimization finite element method for steady convection-diffusion equations, J. Comput. Phys., 425: 109895, 2021.
[23] J. Lv and Y. Li, Optimal biquadratic finite volume element methods on quadrilateral meshes, SIAM J. Numer. Anal., 50: 2379-2399, 2012.
[24] S. Martin, P. Kaufmann, M. Botsch, M. Wicke and M. Gross, Polyhedral finite elements using harmonic basis functions, Comput. Graph. Forum, 27: 1521-1529, 2008.
[25] M. Meyer, A. Barr, H. Lee and M. Desbrun, Generalized barycentric coordinates on irregular polygons, J. Graph. Tools, 7: 13-22, 2002.
[26] P. Milbradt and T. Pick, Polytope finite elements, Int. J. Numer. Meth. Engng., 73: 1811-1835, 2008.
[27] A. Rand, A. Gillette and C. Bajaj, Interpolation error estimates for mean value coordinates over convex polygons, Adv. Comput. Math., 39: 327-347, 2013.
[28] T. Schmidt, Box schemes on quadrilateral meshes, Computing, 51: 271-292, 1993.
[29] N. Sukumar and E. Malsch, Recent advances in the construction of polygonal finite element interpolants, Arch. Comput. Meth. Engng., 13: 129-163, 2006.
[30] N. Sukumar and A. Tabarraei, Conforming polygonal finite elements, Int. J. Numer. Meth. Engng., 61: 2045-2066, 2004.
[31] S. Sun and J. Liu, A locally conservative finite element method based on piecewise constant enrichment of the continuous Galerkin method, SIAM J. Sci. Comput., 31: 2528-2548, 2009.
[32] A. Tabarraei and N. Sukumar, Application of polygonal finite elements in linear elasticity, Int. J. Comput. Methods, 3: 503-520, 2006.
[33] E. Wachspress, A rational finite element basis, Academic Press, New York, 1975.
[34] X. Wang and Y. Li, L^2 error estimates for high order finite volume methods on triangular meshes, SIAM J. Numer. Anal., 54: 2729-2749, 2016.
[35] M. Wicke, M. Botsch and M. Gross, A finite element method on convex polyhedra, Comput. Graph. Forum, 26: 355-364, 2007.

[36] J. Xu and Q. Zou, Analysis of linear and quadratic simplicial finite volume methods for elliptic equations, Numer. Math., 111: 469-492, 2009.

[37] Z. Zhang and Q. Zou, Some recent advances on vertex centered finite volume element methods for elliptic equations, Sci. China Math., 56: 2507-2522, 2013.

[38] Z. Zhang and Q. Zou, Vertex-centered finite volume schemes of any order over quadrilateral meshes for elliptic boundary value problems, Numer. Math., 130: 363-393, 2015.

[39] Y. Zhou and J. Wu, A unified analysis of a class of quadratic finite volume element schemes on triangular meshes, Adv. Comput. Math., 46: 1-31, 2020.

[40] Y. Zhou and J. Wu, High order locally conservative finite element solutions for anisotropic diffusion problems in two dimensions, Comput. Math. Appl., 92: 1-12, 2021.

[41] Y. Zhou and J. Wu, A new high order finite volume element solution on arbitrary triangular and quadrilateral meshes, Appl. Math. Lett., 134: 108354, 2022.

[42] Y. Zhou, Y. Zhang and J. Wu, A polygonal finite volume element method for anisotropic diffusion problems, Comput. Math. Appl., 140: 225-236, 2023.

[43] Q. Zou, L. Guo and Q. Deng, High order continuous local-conserving fluxes and finite-volume-like finite element solutions for elliptic equations, SIAM J. Numer. Anal., 55: 2666-2686, 2017.

Graduate School of China Academy of Engineering Physics, Beijing, 100088, China; Institute of Applied Physics and Computational Mathematics, Beijing, 100088, China

E-mail: `zhangyanlong19@gscaep.ac.cn`

School of Mathematics and Systems Science, Guangdong Polytechnic Normal University, Guang -zhou, 510665, China

E-mail: `zhouyh9@mail2.sysu.edu.cn`